Supplementary Information for

Plasma-induced nitrogen vacancy-mediated ammonia synthesis over a VN catalyst

Shijian Luo[1], Yongduo Liu[1], Yang Song[1], Yuran Yang[1], Fadong Chen[1], Siguo Chen[1,2]*, and Zidong Wei[1,2]

[1] College of Chemistry and Chemical Engineering, Chongqing University, Chongqing, 400044, China.

[2] State Key Laboratory of Advanced Chemical Power Sources (SKL-ACPS), Chongqing, China.

* Corresponding author. Email: csg810519@126.com

The PDF file includes:

Materials and Methods

Materials

Divanadium pentaoxide (99.5%), oxalic acid (99.5%), urea (99%), and methanol (AR) were purchased from Aladdin Chemistry Co., Ltd. Deionized H_2O was obtained via a Millipore system.

Preparation of the VN catalyst

The V_2O_5 precursor was synthesized by a hydrothermal method. Typically, 0.5 mmol V_2O_5 power and 2 mmol oxalic acid ($H_2C_2O_4 \cdot 2H_2O$) were added into 25 mL deionized water and stirred until to obtain a clear solution. 20 mg urea and 10 mL methanol were added with stirring for 30 min and then transferred into 50 mL Teflon-lined stainless-steel autoclave, heated at 180 ℃ for 12 h, and then washed with deionized water several times and dried at 70℃ for 12 hours to obtain V_2O_5 precursor. To prepare the VN catalyst, the V_2O_5 precursor was further placed in the furnace and heated to 700 °C with a heating rate of 5 °C min^{-1} under a flowing NH_3 atmosphere. After heating for 3 h, the system was allowed to cool down to room temperature naturally. The sample above was washed three times in 0.1 M HCl solution to gain the VN catalyst. For comparison, commercial V_2O_5 was used as a precursor to obtain VN nanoparticles through the same process.

Characterizations

X-ray diffraction was performed using an XRD-6000 with Cu Kα radiation at 5°/min. SEM was carried out using a TM-4000 Plus system. TEM and EDX mapping were performed utilizing a Thermo Fisher Scientific Talos F200S system. The lattice distance of the prepared samples was measured employing digital micrograph software. XPS was conducted via a Thermo Fisher Scientific ESCALAB 250Xi system. EPR data were obtained through an EPR200-Plus system. The absorbance was measured via a Shanghai Jingke 752N plus UV–Vis spectrophotometer. Online mass spectrometry (MS) was applied by MS (HIDEN HPR-20).

Experimental Setup

The experimental device for the plasma-catalytic NH_3 synthesis system is shown in Fig. S4. The coaxial DBD reactor comprised a corundum tube and a stainless-steel inner electrode, and a stainless-steel mesh covered the corundum tube as the ground electrode. The input power of the reaction system was controlled by an electric supply device and coupling transformer (purchased from Nanjing Suman Plasma Technology). The average frequency was 10 kHz. An oscilloscope (Tektronix TBS1102) was used to measure the discharge parameter. The voltage on the external capacitor (0.47 μF) was estimated to determine the amount of charge accumulated in the DBD. The length of the discharge region was 15 cm, and the discharge gap was 5 mm. The temperature of the DBD reactor was measured via a thermocouple. The reaction temperature was kept stable by a furnace and fan. The internal pressure of the DBD reactor was maintained at 1 atm. A mixture of N_2 and H_2 was used as the reactant. The gas flow rate was measured via a mass flow meter. When power was input, discharge occurred between the inner electrode and the inner wall of the corundum tube. The synthesized NH_3 was absorbed by the H_2SO_4 solution and then Nessler's reagent method was applied to measure the concentration through a UV–Vis spectrophotometer

(Shanghai Jingke 752N Plus).

Determination of NH_4^+

The concentration of ammonia was determined by Nessler's reagent method. First, 50 mL of absorbent solution was transferred to a 50 mL flask. Then, 1 mL of $KNaC_4H_4O_6$ solution was poured into the flask. After mixing, 1 mL of Nessler's reagent was added to the above flask. The mixture was left to stand for 10 minutes. Finally, the ammonia concentration was determined from UV–Vis absorption spectra at 420 nm by applying a fitting curve for standard concentrations (Fig. S6).

Calculations of the NH_3 synthesis yield and energy efficiency

The NH_3 yield was determined by means of the following equation:

$$v_{NH_3} = \frac{[NH_3] \times V}{t \times m_{cat.}}$$

The energy efficiency in $g \cdot kWh^{-1}$ was determined by means of the following equation:

$$\text{Energy efficiency} = \frac{[NH_3] \times V \times 17}{t \times P}$$

where $[NH_3]$ is the measured concentration of ammonia, V is the volume of the tested solution, t is the time for the reaction, $m_{cat.}$ is the mass of the catalysts, and P is the input power of the DBD plasma reactor.

Supplementary figures

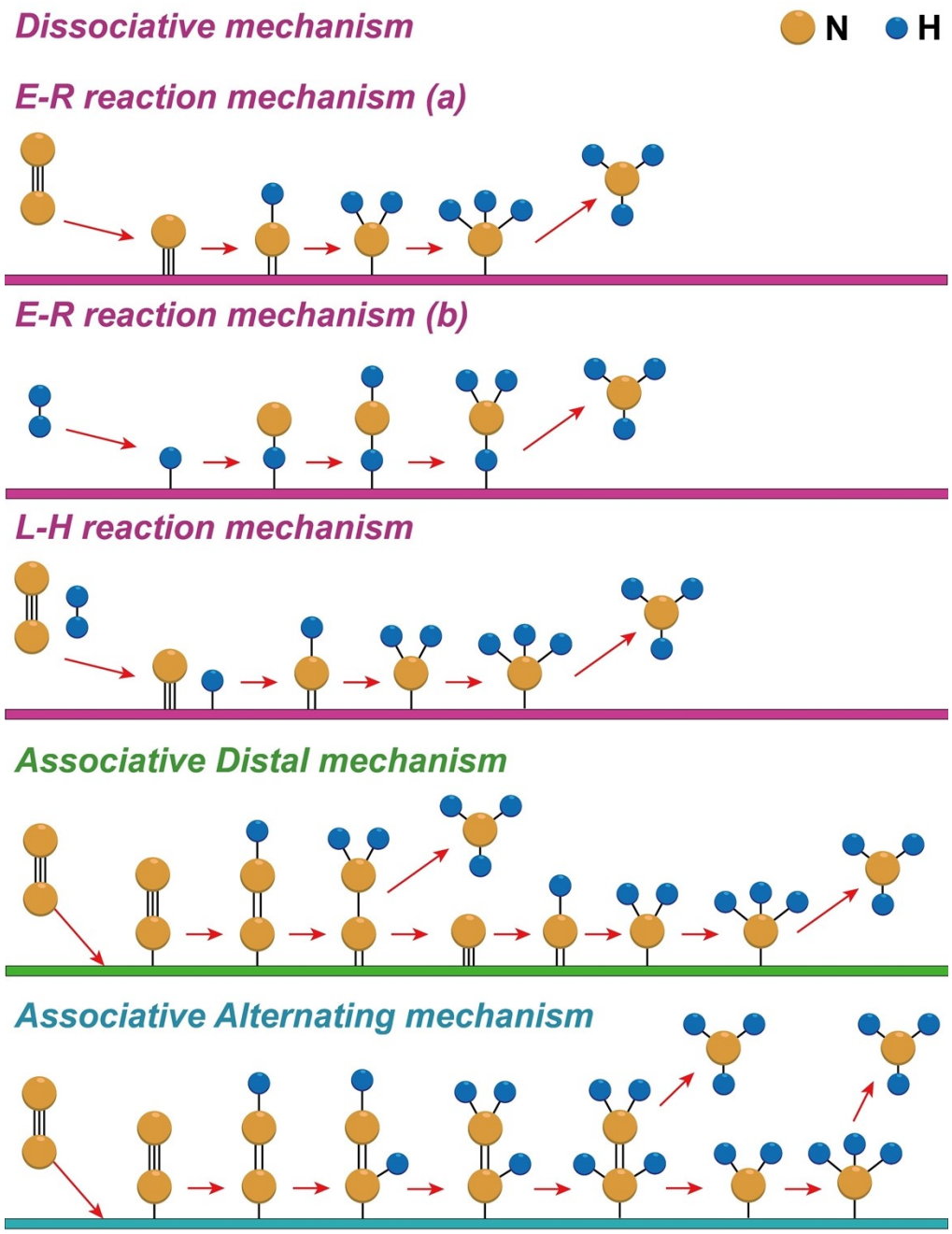

Fig. S1. Schematic diagram for the conventional dissociative and associative mechanisms of NH_3 synthesis on heterogeneous catalysts.

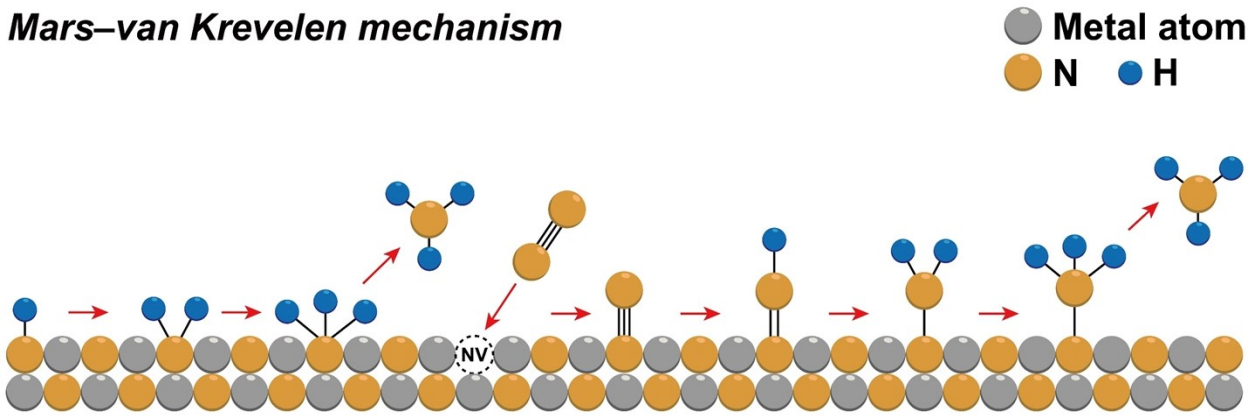

Fig. S2. Schematic diagram for the typical Mars–van Krevelen (MvK) mechanism of NH_3 synthesis on heterogeneous catalysts.

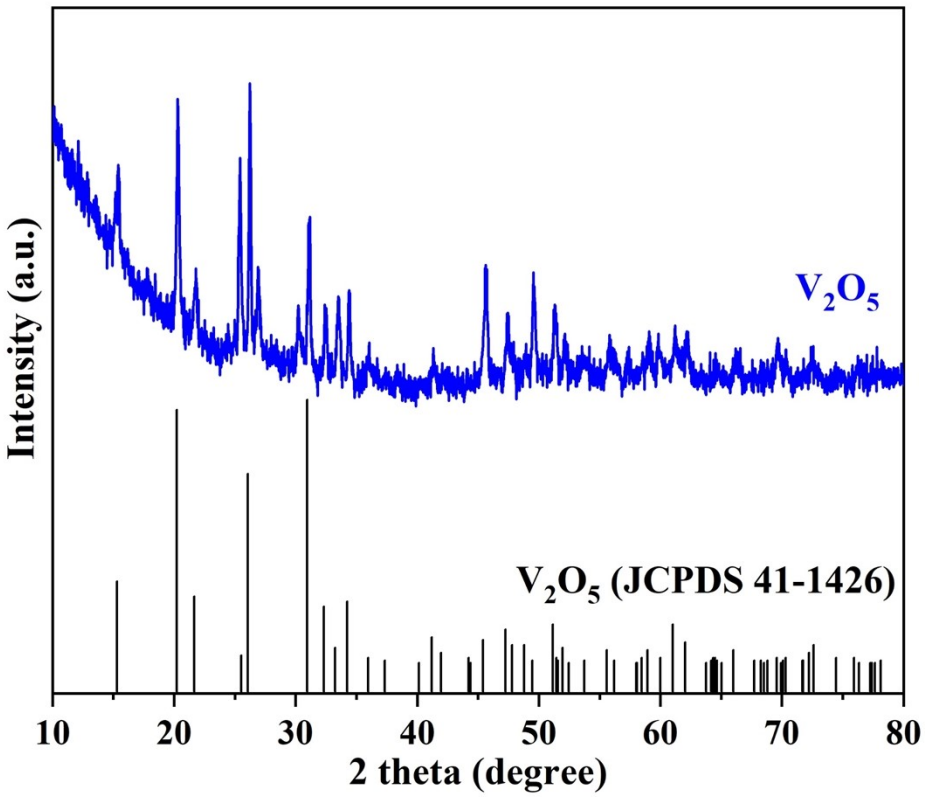

Fig. S3. XRD pattern of V_2O_5 precursor.

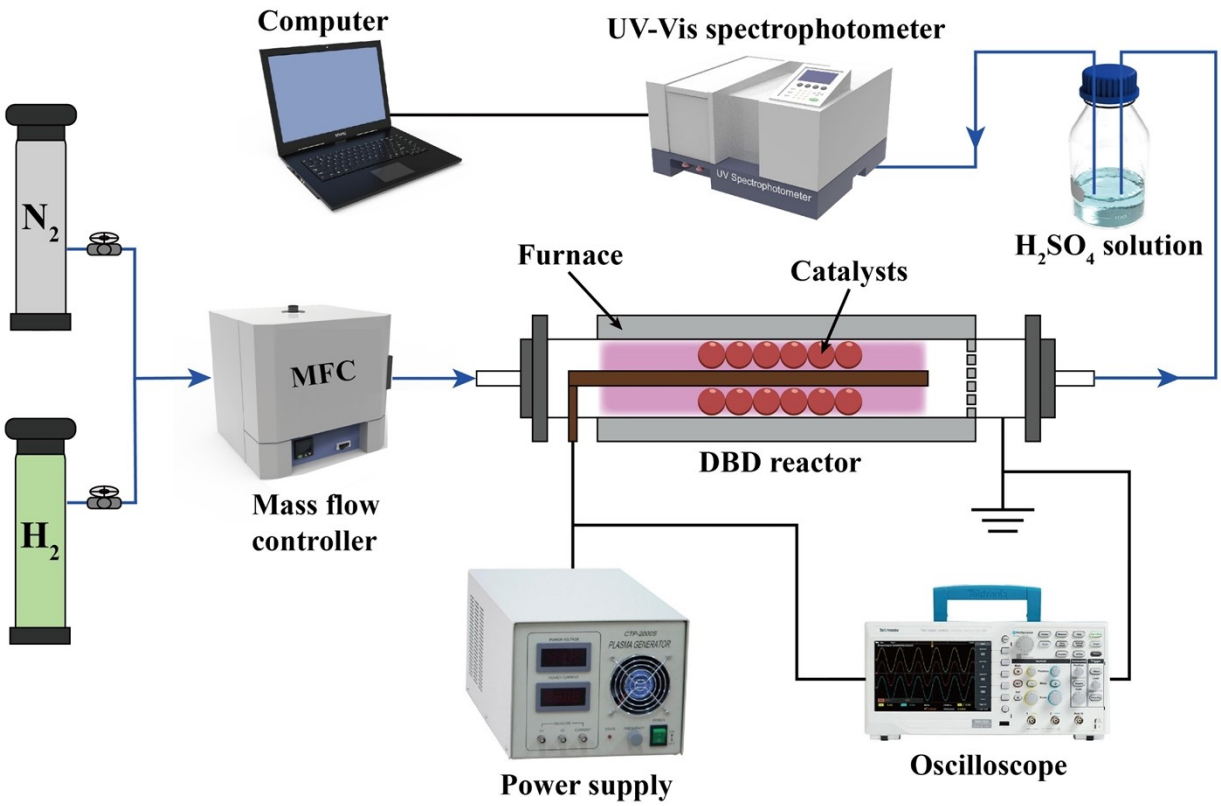

Fig. S4. The experimental device for the plasma-catalytic NH_3 synthesis.

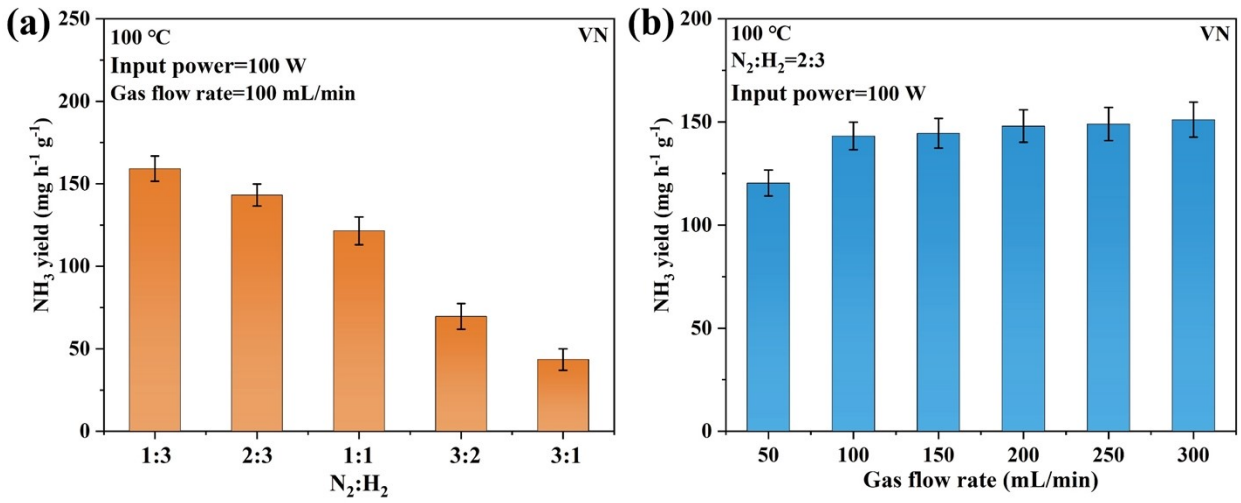

Fig. S5. (a) NH_3 yields at different ratios of N_2 and H_2 over the VN catalyst, (b) NH_3 yields at different gas flow rates over the VN catalyst.

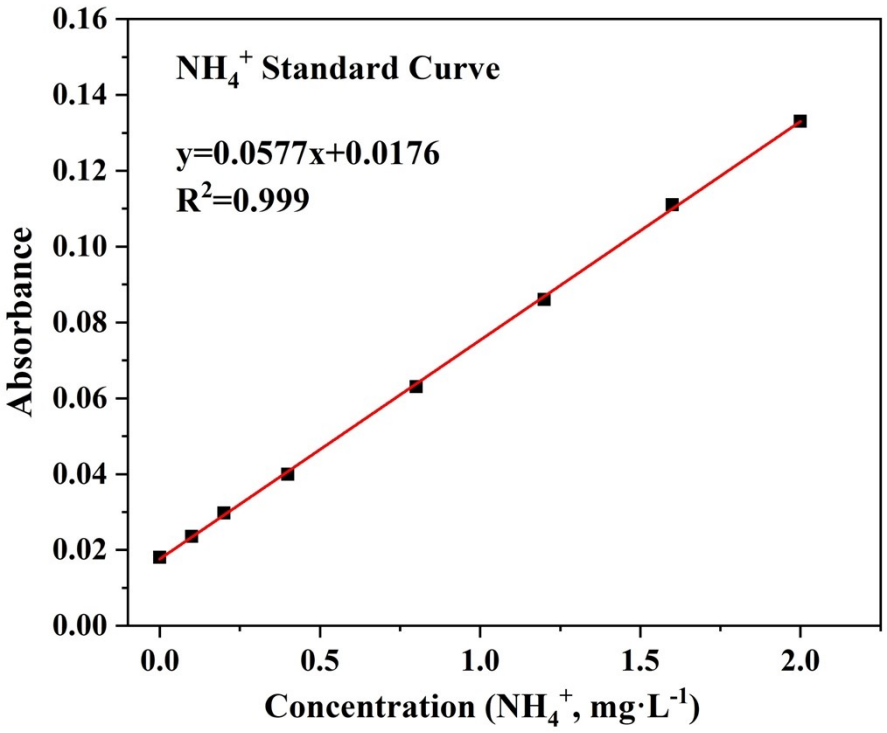

Fig. S6. Concentration–absorbance curve of the NH_4^+ ion solution with a series of standard concentrations. The absorbance at 420 nm was measured via a UV–Vis spectrophotometer.

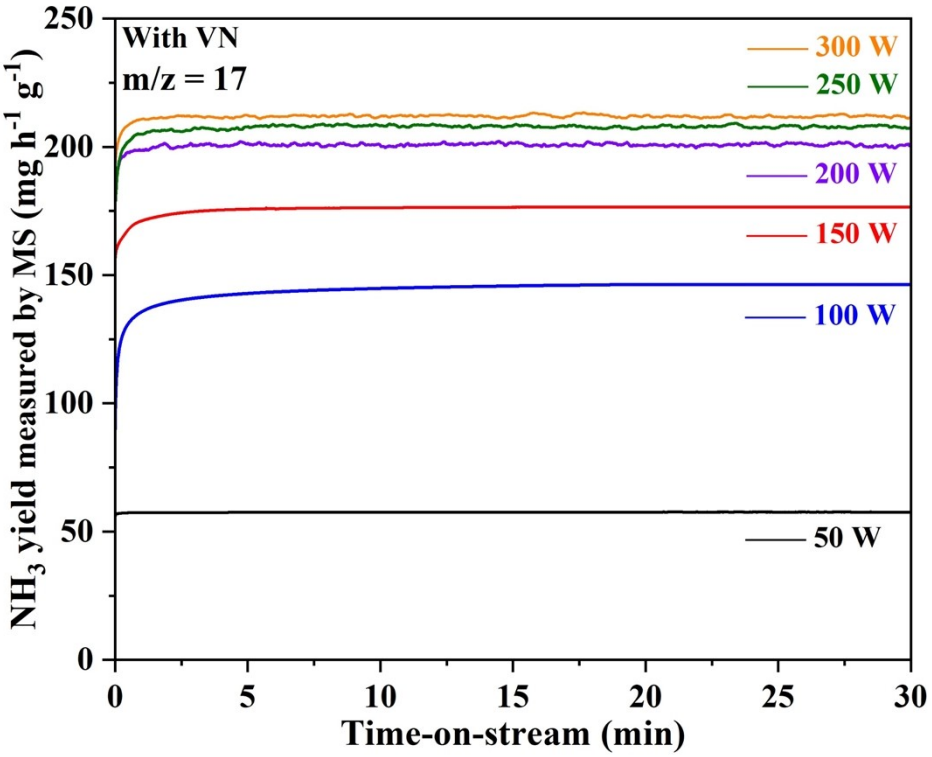

Fig. S7. Online mass spectrometry measurements of NH_3 over the VN catalyst at various input powers.

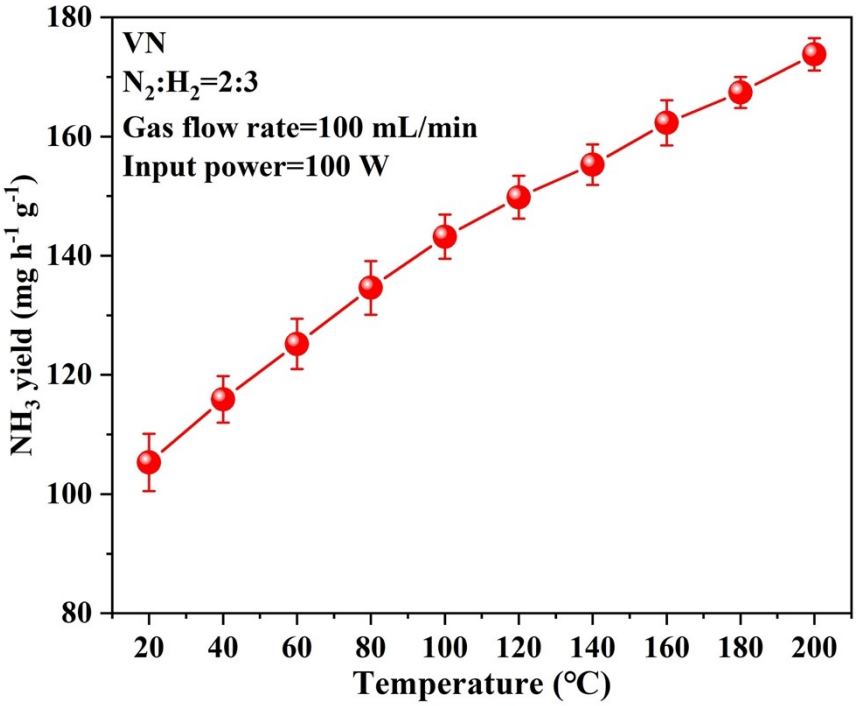

Fig. S8. NH_3 yields of the VN catalyst at temperatures from 293 to 473 K.

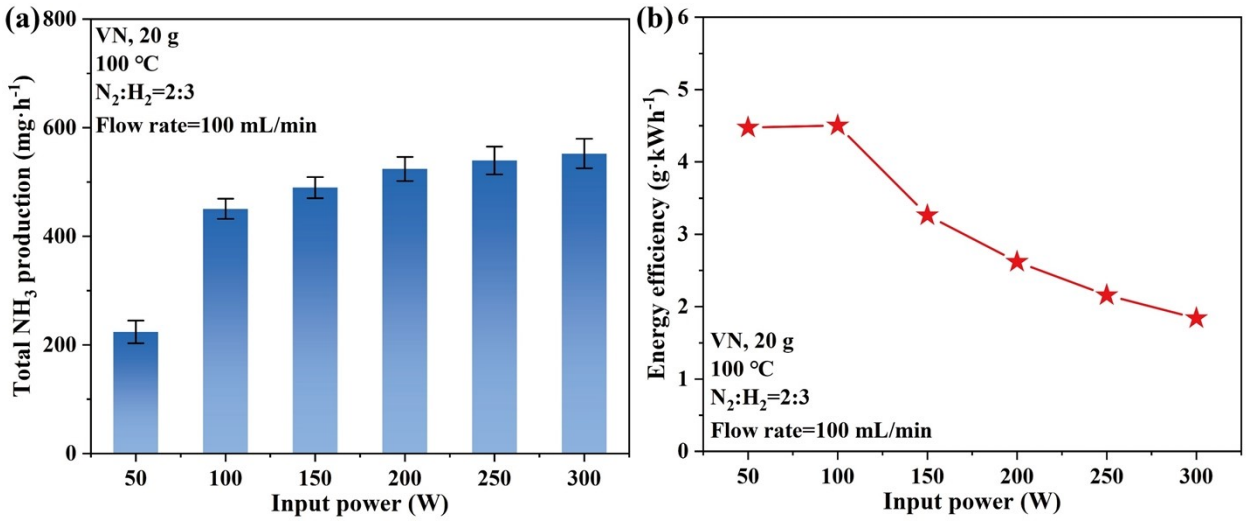

Fig. S9. (a) Total NH_3 productions, and (b) energy efficiencies of 20 g VN catalyst at different input powers.

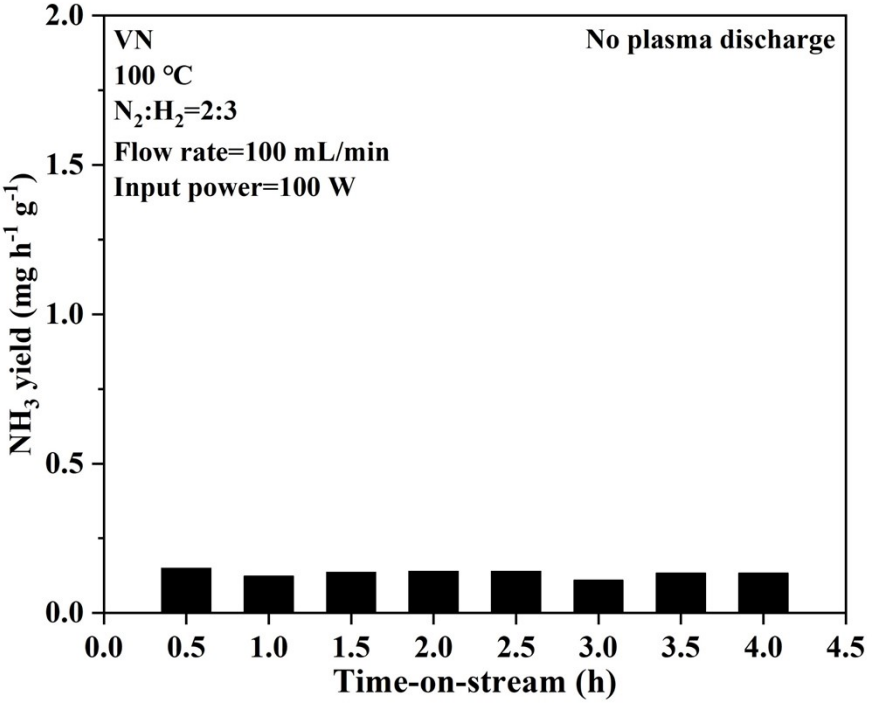

Fig. S10. The performance of ammonia synthesis without plasma discharge.

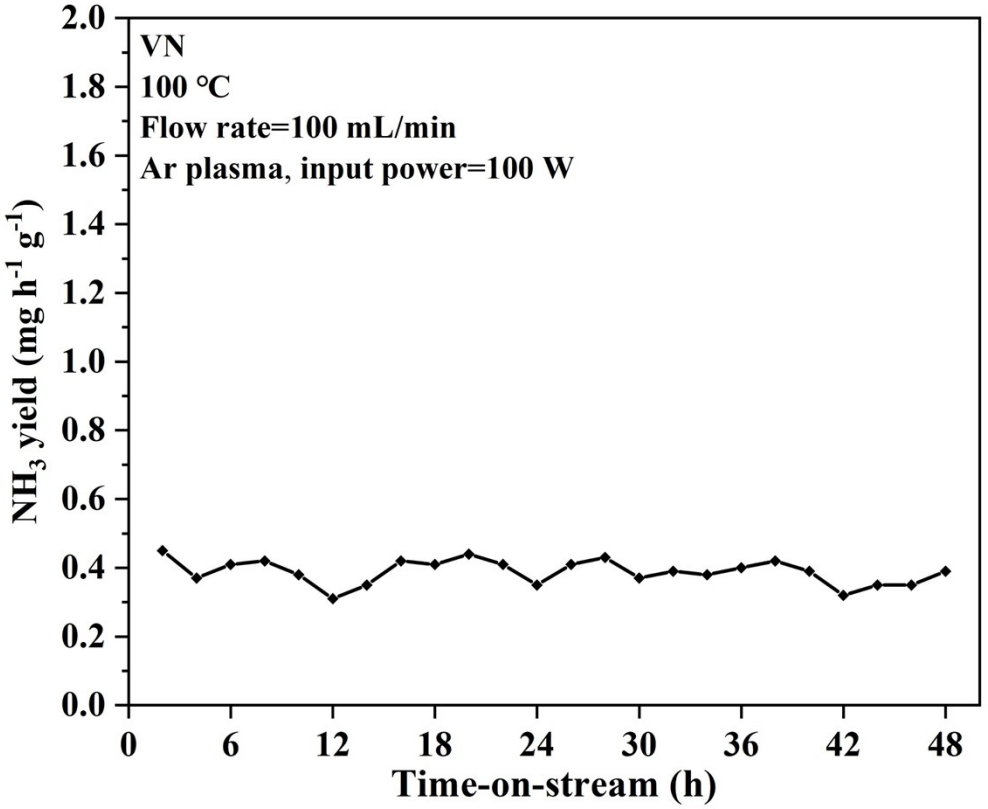

Fig. S11. 48 h plasma-catalytic NH_3 synthesis tests over the VN catalyst under Ar plasma condition.

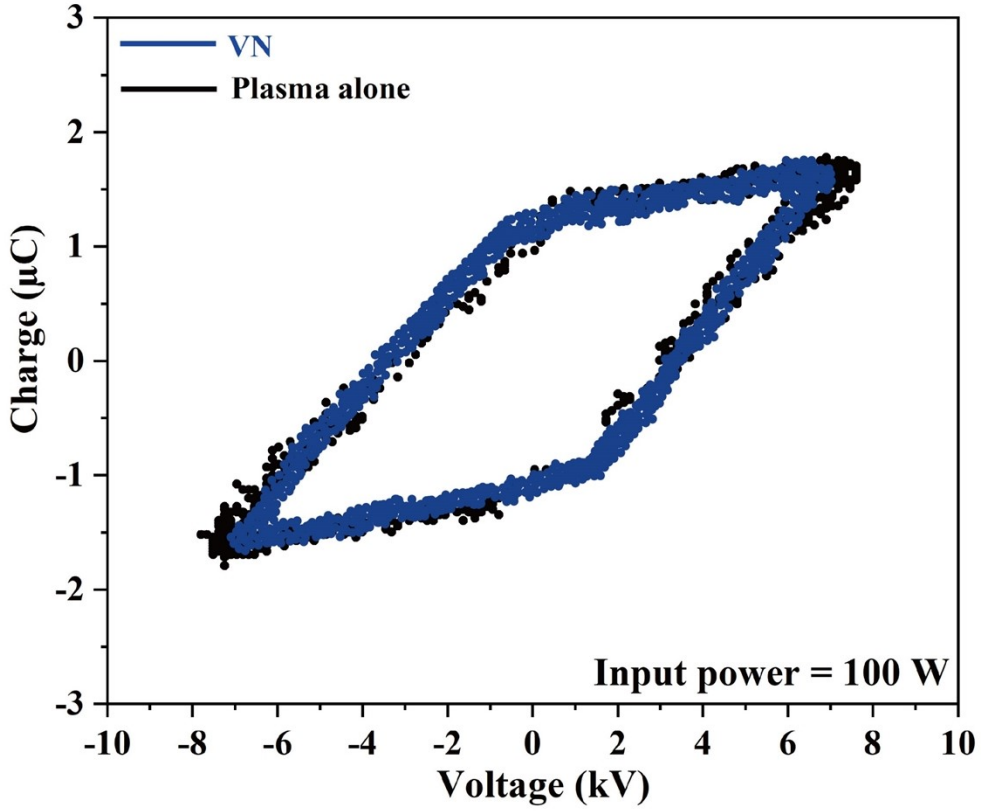

Fig. S12. Lissajous figures of the VN catalyst at the input power of 100 W.

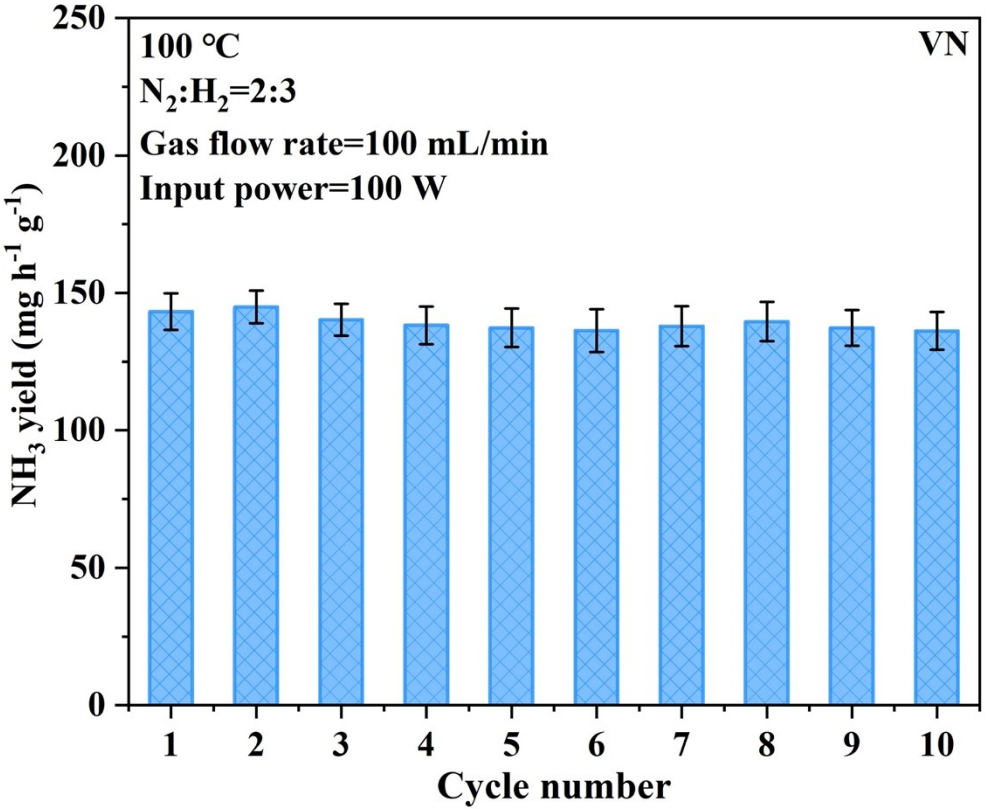

Fig. S13. (a) Cycling test of the VN catalyst with 10 times cycles.

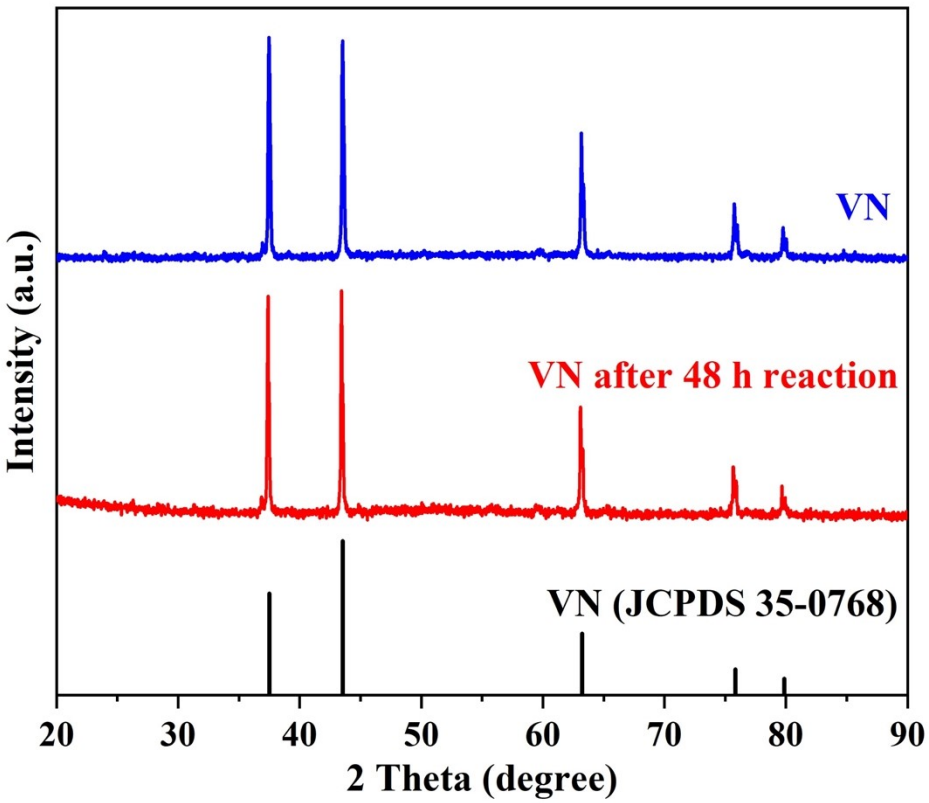

Fig. S14. XRD patterns of the VN catalyst and it after 48 h plasma-catalytic NH_3 synthesis tests.

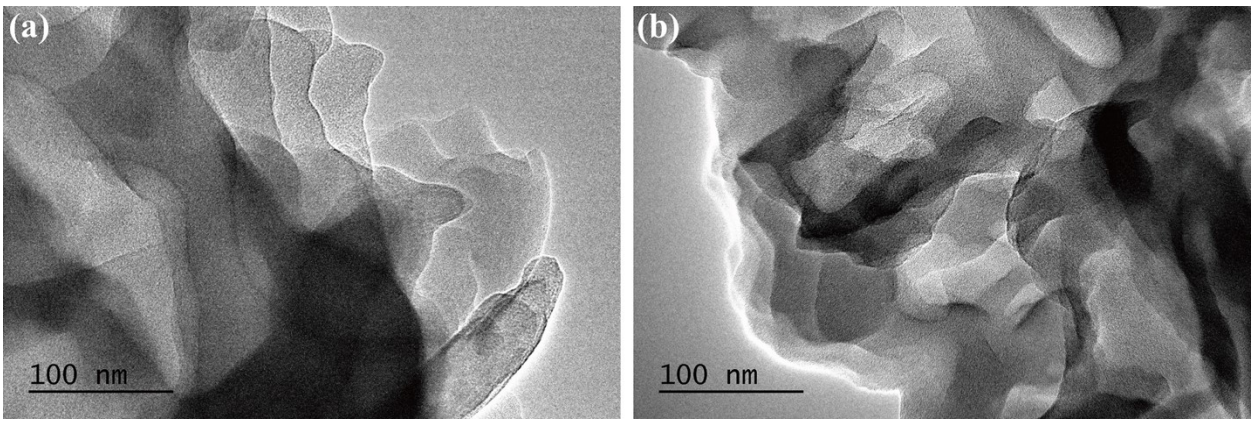

Fig. S15. TEM images of the VN catalyst (a) and it after 48 h plasma-catalytic NH_3 synthesis tests (b).

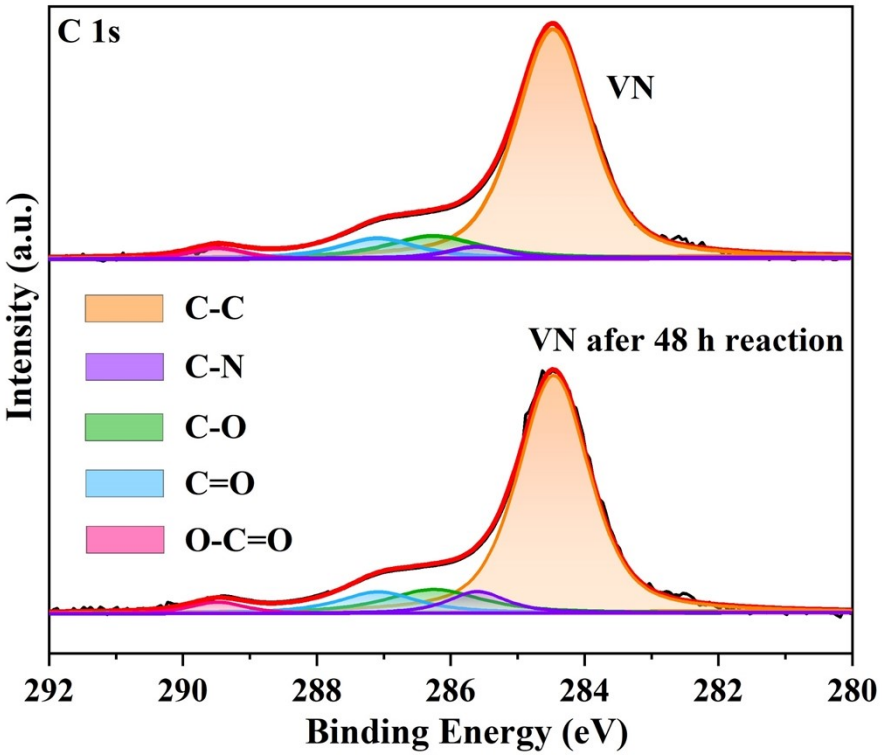

Fig. S16. C 1s XPS spectra of the fresh VN catalyst and it after 48 h reaction.

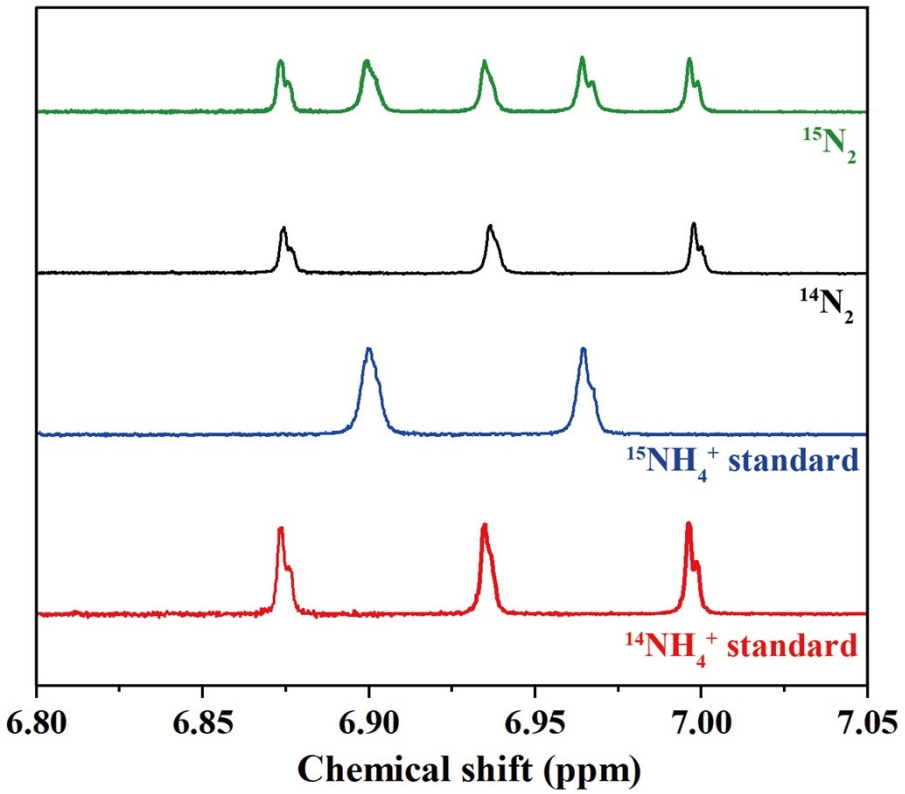

Fig. S17. ^{1}H NMR spectra for $^{14}NH_4^+$ and $^{15}NH_4^+$ standard sample. ^{1}H NMR spectra of ammonia absorption solution after reaction using $^{14}N_2$ and $^{15}N_2$ as the feeding gas.

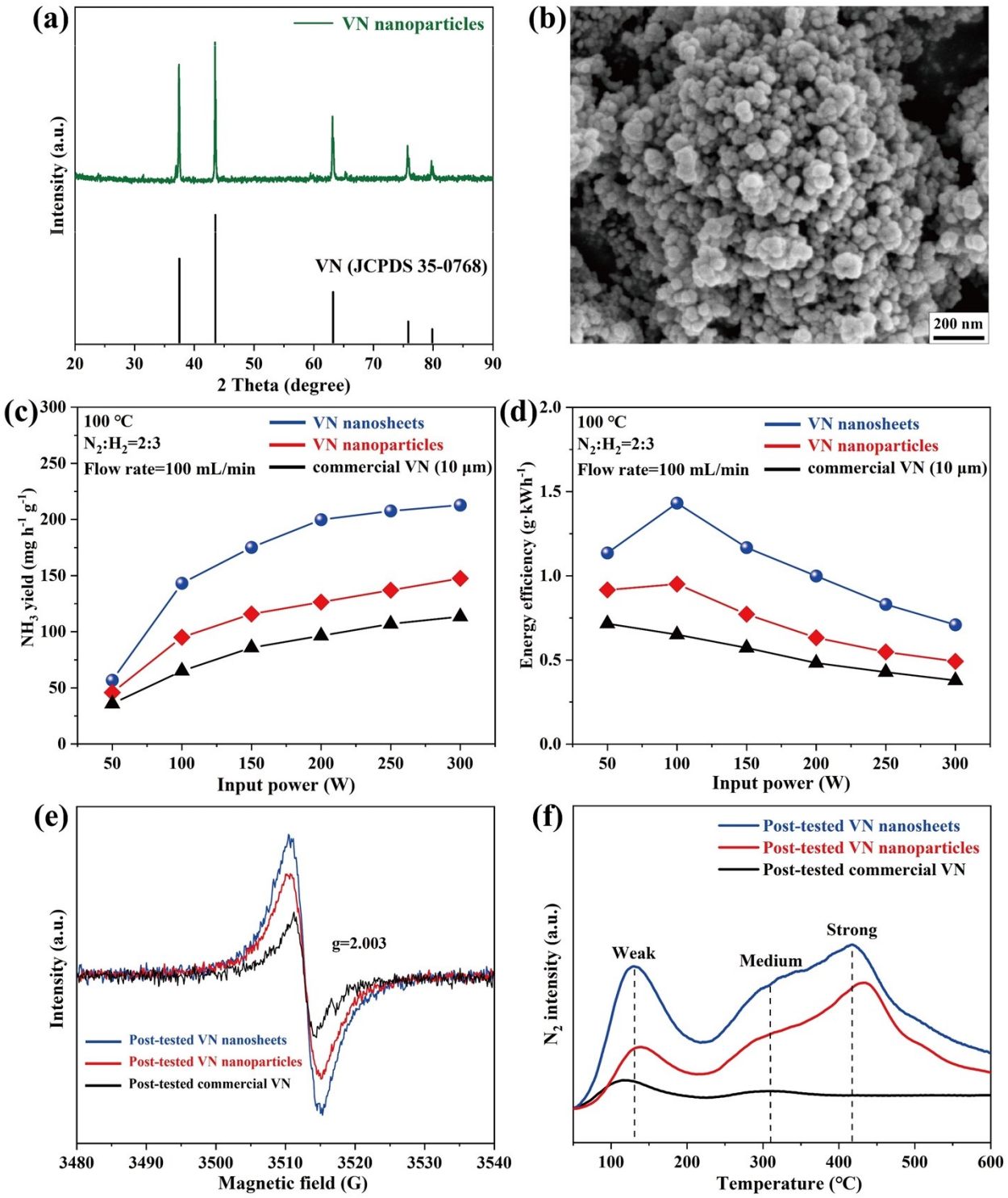

Fig. S18. (a) XRD pattern and (b) SEM image of the VN nanoparticles. (c) NH_3 yields and (d) energy efficiencies of VN nanosheets, VN nanoparticles, and commercial VN (10 μm). (e) EPR results and (f) N_2-TPD profile of the VN nanosheets, VN nanoparticles, and commercial VN (10 μm).

Supplementary tables

Table S1. Comparison of NH_3 yield and energy efficiency for the plasma-catalytic NH_3 synthesis.

Catalyst	Catalyst loading	NH_3 yield ($mg\ h^{-1}\ g^{-1}_{cat.}$)	Energy efficiency ($g_{NH3}\ kWh^{-1}$)	Reference
VN	1 g	143.2	1.43	This work
VN	20 g	22.5	4.50	This work
Ni/Al_2O_3	2 g	8.1	0.29	[1]
$Ru\text{-}Mg/Al_2O_3$	17.1 g	13.6	35.70	[2]
Ni/MgO/ SBA-15	1 g	76.5	1.05	[3]
ZIF-67	0.1 g	43.0	0.24	[4]
$5\%\ Ru/Al_2O_3$	3.6 g	20.2	1.89	[5]
Co SACs	1 g	181	0.31	[6]
Au wire	2.07 g	37.2	0.59	[7]
Ru/Al_2O_3 membrane	0.1 g	16.3	0.37	[8]
MCM-41	0.2 g	24.7	0.5	[9]
NaH-mediated PCLAS	0.05 g	35.4	0.14	[10]
$RuCo/MgTiO_3$	0.2 g	51	1.54	[11]
0.5Ni/LaOF	0.1 g	35.64	2.7	[12]

References

1 Y. Wang, M. Craven, X. Yu, J. Ding, P. Bryant, J. Huang and X. Tu, *ACS Catal.*, 2019, **9**, 10780–10793.

2 H. H. Kim, Y. Teramoto, A. Ogata, H. Takagi and T. Nanba, *Plasma Process. Polym.*, 2017, **14**, 1–9.

3 S. Li, Y. Shao, H. Chen and X. Fan, *Ind. Eng. Chem. Res.*, 2022, **61**, 3292–3302.

4 F. Gorky, J. M. Lucero, J. M. Crawford, B. Blake, M. A. Carreon and M. L. Carreon, *ACS Appl. Mater. Interfaces*, 2021, **13**, 21338–21348.

5 S. Li, T. van Raak and F. Gallucci, *J. Phys. D. Appl. Phys.*, 2020, **53**, 014008.

6 X. Li, Y. Jiao, Y. Cui, C. Dai, P. Ren, C. Song and X. Ma, *ACS Appl. Mater. Interfaces*, 2021, **13**, 52498–52507.

7 M. Iwamoto, M. Akiyama, K. Aihara and T. Deguchi, *ACS Catal.*, 2017, **7**, 6924–6929.

8 T. Mizushima, K. Matsumoto, J. I. Sugoh, H. Ohkita and N. Kakuta, *Appl. Catal. A Gen.*, 2004, **265**, 53–59.

9 Y. Wang, W. Yang, S. Xu, S. Zhao, G. Chen, A. Weidenkaff, C. Hardacre, X. Fan, J. Huang and X. Tu, *J. Am. Chem. Soc.*, 2022, **144**, 12020–12031.

10 H. Wu, L. Yang, J. Wen, Y. Xu, Y. Cai, W. Gao, Q. Wang, Y. Guan, S. Feng, H. Cao, T. He, L. Liu, S. Zhang, J. Guo and P. Chen, *Adv. Energy Mater.*, 2023, **13**, 2300722.

11 Y. Zhang, S. Li, Z. Yuan, H. Chen and X. Fan, *Ind. Eng. Chem. Res.*, 2022, **61**, 14199–14210.

12 K. Li, S. Chen, H. Wang and F. Wang, *Appl. Catal. A Gen.*, 2023, **650**, 118983.